PNAS RESEARCH ARTICLE | APPLIED PHYSICAL SCIENCES

Wettability-based ultrasensitive detection of amphiphiles through directed concentration at disordered regions in self-assembled monolayers

Yuxing Yao[a,1], Robert K. A. Bennett[b,1], Yang Xu[c], Adil M. Rather[c], Shucong Li[a], Tung Chun Cheung[b], Alisha Bhanji[b], Michael J. Kreder[b], Dan Daniel[b,d], Solomon Adera[b], Joanna Aizenberg[a,b,2], and Xiaoguang Wang[c,e,2]

Contributed by Joanna Aizenberg; received June 27, 2022; accepted September 21, 2022; reviewed by Howard Stone, Paul Weiss, and Aleksandr Noy

Various forms of ecological monitoring and disease diagnosis rely upon the detection of amphiphiles, including lipids, lipopolysaccharides, and lipoproteins, at ultralow concentrations in small droplets. Although assays based on droplets' wettability provide promising options in some cases, their reliance on the measurements of surface and bulk properties of whole droplets (e.g., contact angles, surface tensions) makes it difficult to monitor trace amounts of these amphiphiles within small-volume samples. Here, we report a design principle in which self-assembled monolayer–functionalized microstructured surfaces coated with silicone oil create locally disordered regions within a droplet's contact lines to effectively concentrate amphiphiles within the areas that dominate the droplet static friction. Remarkably, such surfaces enable the ultrasensitive, naked-eye detection of amphiphiles through changes in the droplets' sliding angles, even when the concentration is four to five orders of magnitude below their critical micelle concentration. We develop a thermodynamic model to explain the partitioning of amphiphiles at the contact line by their cooperative association within the disordered, loosely packed regions of the self-assembled monolayer. Based on this local analyte concentrating effect, we showcase laboratory-on-a-chip surfaces with positionally dependent pinning forces capable of both detecting industrially and biologically relevant amphiphiles (e.g., bacterial endotoxins), as well as sorting aqueous droplets into discrete groups based on their amphiphile concentrations. Furthermore, we demonstrate that the sliding behavior of amphiphile-laden aqueous droplets provides insight into the amphiphile's effective length, thereby allowing these surfaces to discriminate between analytes with highly disparate molecular sizes.

sensors | amphiphiles | wettability | self-assembly | lubricated surfaces

Significance

Wettability-based molecular detection is emerging to enable portable and fast chemical detection within droplets. However, current detection methods can only respond to changes in a droplet's bulk wetting properties, leading to poor detection limits. We report a design principle that overcomes this fundamental limitation by locally concentrating analytes within a droplet's contact line to modulate the local surface roughness, which further affects droplet mobility. This mechanism enables the detection of molecules even at minute concentrations where droplets' bulk wetting properties are unchanged. This design can be implemented to functional surface devices that can readily sort microliter aqueous droplets into discrete groups with different amphiphile concentrations and molecular sizes, which have potential for early disease diagnostics and environmental water quality monitoring.

Amphiphiles, molecules composed of both polar and apolar moieties, are a large class of chemicals that can self-assemble at interfaces and give rise to measurable changes of surface properties at concentrations close to their critical micelle concentrations (CMCs). During the past several decades, studies have demonstrated that biological amphiphiles can affect both ecological and biological functions even at concentrations significantly below their CMC (1, 2). The detection of minute amphiphile concentrations can therefore be used to monitor the condition of biological systems (3–12). For instance, various diseases can be diagnosed or monitored by measuring the concentration of amphiphilic biomarkers, including lipoarabinomannan and carbohydrate antigen 15-3, for early-stage tuberculosis (7, 8) and cancer prognosis (1, 13), respectively. Reliable and sensitive detection of various important biological amphiphiles, such as endotoxins secreted by Gram-negative bacteria (e.g., *Escherichia coli*), can also provide important information on water and food safety. For instance, consumption of water that contains endotoxins at concentrations as low as 2 ng/mL, four orders of magnitude below its CMC, may induce sepsis in humans (14, 15). Monitoring the concentration of endotoxins is conventionally achieved using the limulus amebocyte lysate assay, which relies upon blood extracted from the horseshoe crab, posing unique ecological and ethical concerns (16). Recently, assays based on responsive materials such as liquid crystals and fluorescent proteins have been developed to detect low concentrations of endotoxins (17–20). However, these assays rely upon the use of specialized chemicals and equipment, making these tests unsuitable for portable and fast on-site or point-of-care amphiphile detection.

Recently, wettability-based assays have shown potential for detecting various analytes by exploiting the wetting properties of liquid samples on functional surfaces. Specifically, visually examining the mobility of aqueous droplets can serve as a fast and accessible method to determine the concentration of amphiphilic analytes in water, ranging

Reviewers: H.A.S., Princeton University; P.S.W., University of California, Los Angeles; and A.N., Lawrence Livermore National Laboratory.

The authors declare no competing interest.

See online for related content such as Commentaries.

[1]Y.Y. and R.K.A.B. contributed equally to this work.

[2]To whom correspondence may be addressed. Email: jaiz@seas.harvard.edu or wang.12206@osu.edu.

This article contains supporting information online at http://www.pnas.org/lookup/suppl/doi:10.1073/pnas.2211042119/-/DCSupplemental.

Published October 17, 2022.

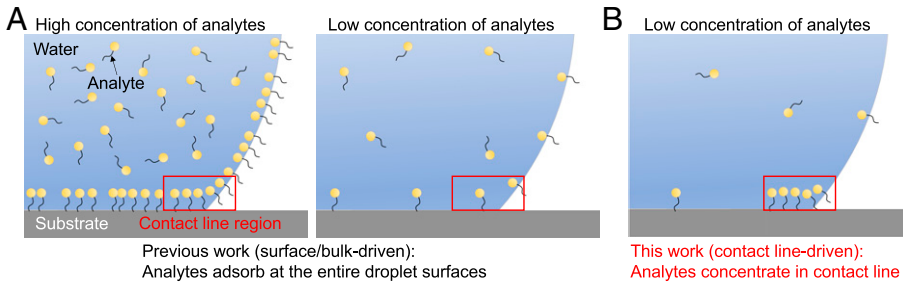

Scheme 1. Comparison between mechanisms involved in amphiphile detection using wettability-based sensors. (*A*) Traditional wettability-based sensors rely on the partitioning of analytes between the bulk phase and on the surface of water droplets to induce changes in the droplets' surface tension. At low concentrations of analytes, the surface tension of aqueous droplets is indistinguishable from that of pure water. (*B*) Proposed contact line–based sensors take advantage of the local concentration of analyte molecules via their preferential partition within a contact line region, which may lead to different sliding behaviors from those of pure water even at trace amounts of analytes in water droplets. Red boxes indicate the contact line region. The distribution of analyte molecules is schematic.

from synthetic amphiphiles to organic solvents (21–24). Although these assays enable naked-eye detection without using specialized equipment, they generally rely on significant changes of the surface tension of the entire water droplet. Consequently, wettability assays are rarely applied to detect amphiphiles at concentrations more than two orders of magnitude lower than their CMC, at which no measurable changes to the surface tension (e.g., as measured by contact angle goniometry) occur, as illustrated in Scheme 1*A*. For biologically related surfactants (e.g., endotoxin), the CMC is generally tens of micrograms per milliliter (25), making their detection even more challenging with wettability-based methods.

It is well established that the mobility of water droplets on surfaces is dominated by the friction around a droplet's contact line (26–31). This friction is determined not only by the surface tension of the droplet but also by the local roughness of the surface under the contact lines. Therefore, if amphiphiles could become locally concentrated around the contact line of a droplet, an opportunity would arise to detect the amphiphiles based on the droplet's pinning forces and so-induced sliding behavior—even if the amphiphile's bulk concentration could cause no measurable changes to the bulk surface tension of the underlying droplet (Scheme 1*B*). Such a possibility of selective partition of amphiphiles in contact line regions, however, has not yet been explored.

Here, we demonstrate a design principle that relies upon concentrating amphiphiles into a droplet's contact lines to enable their ultrasensitive detection by visually inspecting droplets' sliding angles. Specifically, we find that self-assembled monolayer (SAM)–functionalized, lubricant-infused microstructured surfaces can selectively concentrate amphiphiles inside water droplets at the disordered, loosely packed SAM regions—which largely overlap with the droplet's contact line—to generate pinning forces, and therefore significantly affect the mobility of analyte-containing droplets on our functional surfaces. Interestingly, we observe that the changes in droplets' pinning forces remain easily measurable even when the concentration of amphiphiles is as low as five orders of magnitude below the amphiphile's CMC, where the surface tension is essentially unchanged. Furthermore, we develop a thermodynamic model to describe the essential change in the concentration-dependent cooperative association with the loosely packed molecules in an SAM. In addition, our system can offer insight into the analyte amphiphiles' chemical structures (e.g., molecular size, amphiphilicity) based on the change in static friction experienced by amphiphile-laden droplets. To the best of our knowledge, a similar chemical classification of analytes has not been achieved in conventional surface tension-based techniques. Finally, we demonstrate that introducing a spatial gradient of the contact line's length, which we achieve by exploiting patterned microstructures, allows our surfaces to readily sort aqueous droplets into discrete groups based on their amphiphile concentrations. Our results provide design principles for ultrasensitive, naked-eye detection of both industrially and biologically significant amphiphiles (e.g., bacterial endotoxins) at detection limits that are relevant for ecological monitoring and water and/or food safety.

Results and Discussion

In this work, we aim to engineer the local roughness of contact lines of aqueous droplets on surfaces by concentrating amphiphiles from the bulk of a droplet into its contact line, resulting in measurable changes to droplet mobility at extremely low concentrations of amphiphiles. Previous studies have demonstrated that the ordering of SAMs on topographically patterned surfaces is significantly diminished at the edges relative to flat regions, which facilitates molecular adsorption, droplet pinning, selective etching, and crystal nucleation at these disordered SAM sites (32, 33). Because these disordered regions are generally characterized by loose molecular packing of the constituent silane (34–37) (see schematics in Fig. 1*A*), we anticipated that amphiphile molecules may locally coassemble with SAMs at such sites. (We refer readers to the section "Insights into the Imperfections in SAMs for Amphiphile Self-Assembly" in the *SI Appendix* for a discussion regarding the origin of the disordered regions in the SAM.) To create SAMs with engineered regions of disorder, we fabricated structured surfaces on silicon (Si) wafers with cylindrical micropillars arranged in square arrays, described by their radius (R), pitch (center-to-center spacing, P), and height; the Si micropillar arrays were subsequently functionalized with an SAM of dimethyloctadecyl [3-(trimethoxysilyl)propyl] ammonium chloride (DMOAP) (Fig. 1*A*).

The DMOAP SAM-functionalized microstructures were spin coated with a 10-cSt silicone oil lubricant to create a lubricious liquid overlayer to prevent water droplets from wetting the top surface of Si micropillars. Therefore, we expect that silicone oil–infused, DMOAP-functionalized Si micropillar arrays behave as slippery liquid-infused porous surfaces (SLIPS), with integrated pinning regions defined by the disordered DMOAP SAM around the top edges of micropillars (38). Unless specified otherwise, the volume of droplets of water used in our experiments was 2 μL and the pillar height was fixed at 30 μm to adequately enlarge the surface area of the pillars and sufficiently stabilize a continuous layer of silicone oil on the surface—$R = 5$ μm and $P = 25$ μm.

Fig. 1*B* and *SI Appendix*, Fig. S1 show representative micrographs of a 2-μL water droplet resting on our designed surface

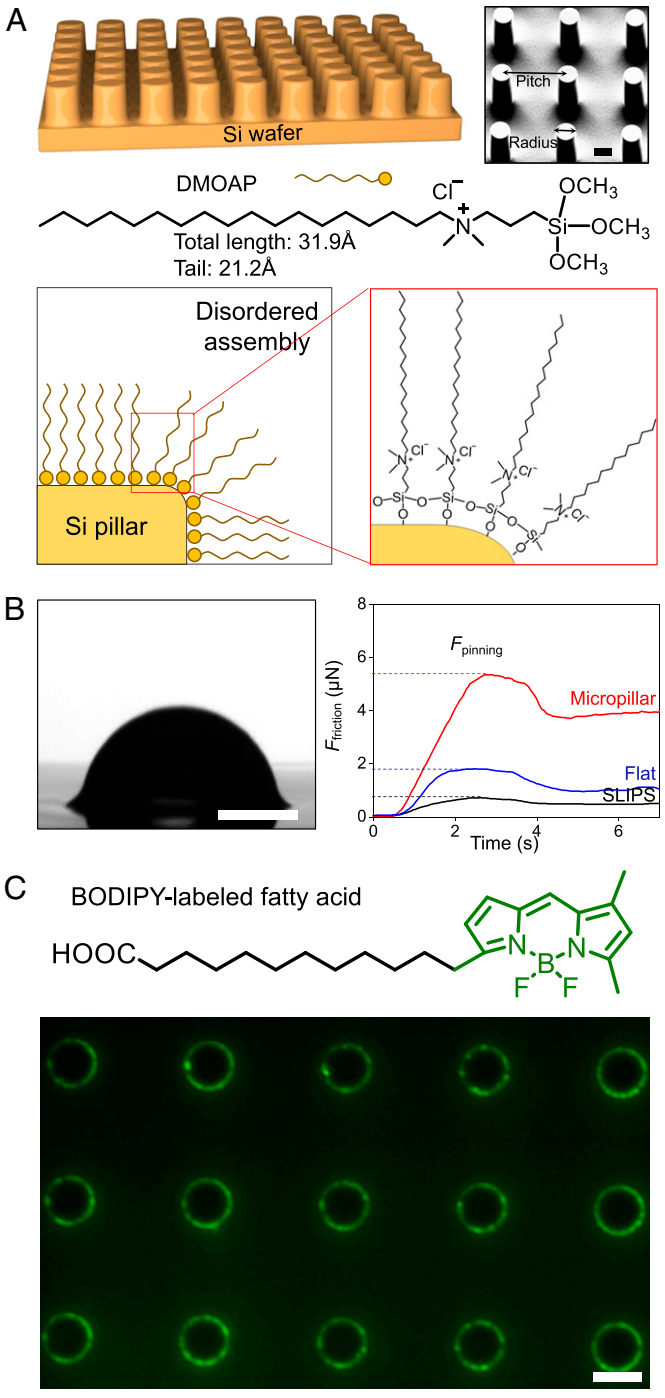

Fig. 1. Design of DMOAP SAM-functionalized, silicone oil–infused Si micropillar arrays that enable cooperative self-assembly of amphiphiles in disordered regions of the SAM at the top edge of the micropillars. (*A*) Schematic illustration of a DMOAP SAM-functionalized Si micropillar array. Disordered DMOAP assembly regions are located at the edge of micropillars. Pillar height, radius, and pitch are fixed at 30 μm, 5 μm, and 25 μm, respectively. Inset shows a representative scanning electron microscopy (SEM) image of micropillar structures on a Si wafer. The length of the DMOAP molecule was calculated from Chem3D. Note that the structure of the SAM is schematic. (*B*) *Left*: A representative goniometer image of a water droplet resting on a DMOAP SAM-functionalized, silicone oil–infused Si micropillar array. *Right*: The friction force experienced by a 2-μL aqueous droplet as a function of time on a DMOAP SAM-functionalized, silicone oil–infused Si micropillar array (red), a flat DMOAP SAM-functionalized, silicone oil–infused flat Si surface (blue), and a conventional SLIPS system with poly(C_4F_8)-functionalized glass coated with Krytox 103 perfluoropolyether lubricant (black). The maximum friction force is defined as the static pinning force, $F_{pinning}$. Scale bar, 500 μm. (*C*) Fluorescence micrograph showing BODIPY-labeled amphiphiles becoming locally concentrated by self-assembling with DMOAP in disordered regions of the SAM at the top edge of the micropillars lubricated with silicone oil. Scale bar, 10 μm.

with an apparent equilibrium contact angle of 86 ± 5°. We measured the typical dissipative forces $F_{friction}$ acting on aqueous droplets sliding across the surface using a custom-built cantilever setup (see Materials and Methods). These values were compared to $F_{friction}$ for water droplets resting on flat DMOAP-functionalized silicone oil–coated surfaces and poly(C_4F_8)-functionalized glass surfaces coated with fluorinated oil (a conventional SLIPS) (39). As shown in Fig. 1*B*, 2-μL water droplets on fluorinated lubricant-based SLIPS and flat DMOAP-functionalized silicone oil–coated Si surfaces experience static force barriers $F_{pinning}$ ~0.9 ± 0.2 and 2.0 ± 0.2 μN, respectively. Water droplets resting on DMOAP SAM-functionalized, silicone oil–infused micropillar arrays, however, need to overcome a much larger $F_{pinning}$ ~5.6 ± 0.4 μN before droplets begin to slide. To remain in motion, these droplets must be continuously detached from micropillars around their receding contact lines, resulting in a dynamic force barrier. The presence of distinct and significant static and dynamic force barriers indicates that water droplets follow a stick–slip mode on our micropillar surfaces, which arises from the displacement of the oil and pinning at the underlying solid (40, 41). Such pinning at the contact lines of surface-bound water droplets overlaps with the highly disordered SAMs of DMOAP around the top edges of micropillars, as we demonstrate by the localized adsorption of aliphatic fatty acids labeled with dipyrromethene boron difluoride (BODIPY) (see Materials and Methods). As shown in Fig. 1*C*, the fluorescence from BODIPY-labeled fatty acids was more intense in the outer edge region at the top surface of the micropillar than both other regions of the Si micropillars and the bulk solution, suggesting that the disordered region in the DMOAP SAM can locally concentrate BODIPY molecules.

From our observations, we reason that the adsorption of amphiphiles at the edges of the microstructures concentrates them at the contact line, thus changing the local (molecular) surface roughness and consequently modifying $F_{pinning}$ of amphiphile-containing aqueous droplets. Indeed, we observe three scenarios of how amphiphiles may affect local disorders that result in three unique effects on $F_{pinning}$.

We tested the anionic surfactant sodium dodecyl sulfate (SDS; Fig. 2*A*), which has a smaller molecular length (4.6 Å head and 13.7 Å tail) than DMOAP (21.2 Å tail). As shown in Fig. 2*B*, the $F_{pinning}$ of 2 μL aqueous droplets on DMOAP SAM-functionalized, silicone oil–infused microstructured surfaces depends strongly on the concentration of SDS. When the concentration of SDS was <100 nM, $F_{pinning}$ of droplets was constant at 5.6 ± 0.4 μN. However, as the concentration of SDS increased to 100 nM, $F_{pinning}$ decreased to 4.2 ± 0.2 μN and continued to gradually decrease to 3.1 ± 0.3 μN as the concentration of SDS increased to 100 μM. We note here that our system shows a measurable decrease in $F_{pinning}$ and sliding angle (*SI Appendix*, Fig. S2) of the droplet at SDS concentrations as low as ~100 nM, which is nearly five orders of magnitude lower than the CMC of SDS (8.2 mM). Similar behavior was observed for the cationic surfactant hexadecyltrimethylammonium bromide (CTAB), which has a length similar to that of SDS. However, the threshold concentration of CTAB appears to be slightly different from that of SDS, as shown in *SI Appendix*, Fig. S3. Such high sensitivity cannot be achieved by previously developed wettability-based sensors that cannot locally concentrate analytes to relevant regions. Instead, traditional designs detect and/or sort aqueous droplets solely based on their reliance on the differences in droplets' surface tensions, which remain largely unchanged at amphiphile concentrations

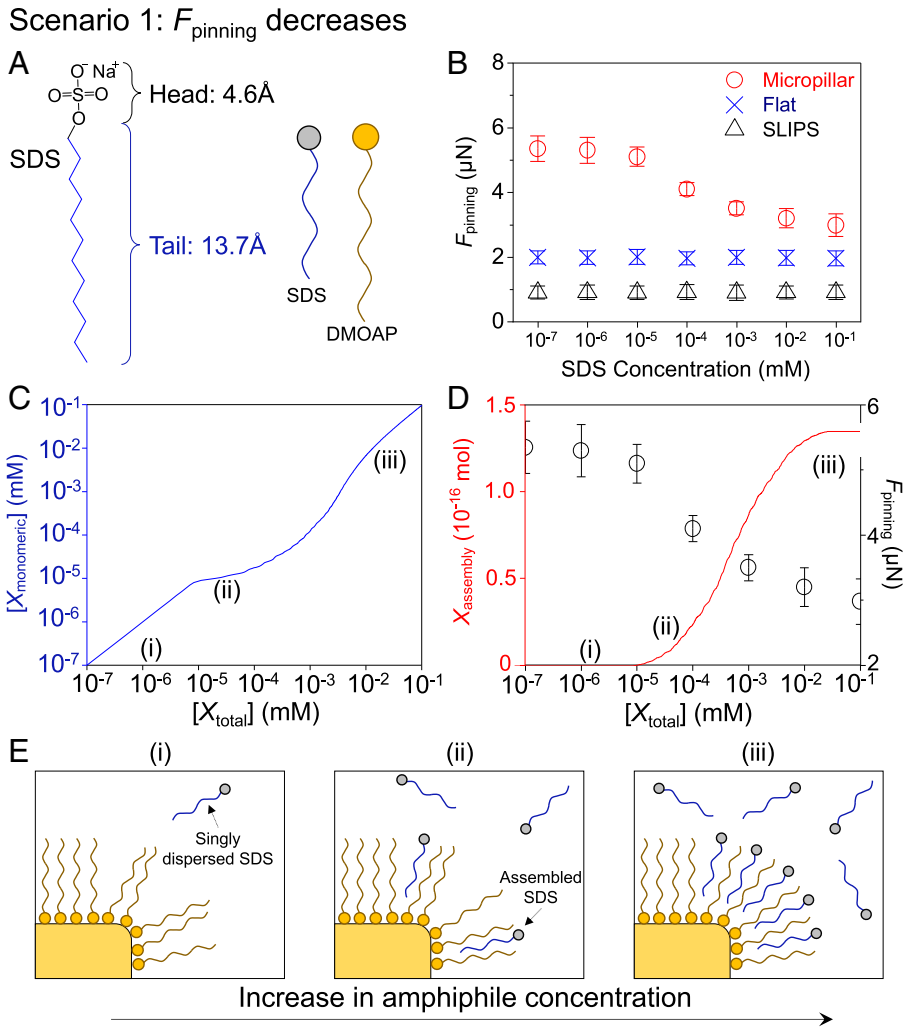

Fig. 2. Effect of amphiphiles' molecular structure on static friction of aqueous droplets on a lubricated DMOAP SAM-functionalized Si micropillar array. (*A*) Molecular structure of SDS. The length of SDS was calculated from Chem3D. (*B*) $F_{pinning}$ of aqueous droplets as a function of SDS concentration on a DMOAP-functionalized Si micropillar array lubricated with silicone oil (red), a DMOAP-functionalized, silicone oil–coated flat Si surface (blue), and a conventional SLIPS system with poly(C_4F_8)-functionalized glass coated with Krytox 103 perfluoropolyether lubricant (black). The volume of aqueous droplets is 2 μL. (*C*, *D*) Dependence of the concentration of (*C*) individually dispersed SDS within water droplets ($X_{monomeric}$) and (*D*) self-assembled SDS within the disordered region of the SAM ($X_{assembly}$) on the total concentration of SDS (X_{total}), as calculated by Eq. 2. The right y axis of (*D*) shows the $F_{pinning}$ of aqueous droplets as a function of total concentration of SDS. Regions (i), (ii), and (iii) correspond to stages depicted in (*E*). (*E*) Schematic illustration of the three stages of cooperative self-assembly of amphiphiles within disordered DMOAP SAM at the top edge of the micropillars as a function of amphiphile concentration. Note that the structure of the SAM is schematic.

below CMC (see below for a detailed discussion). For example, nonlubricated nano-textured surfaces can be used to sense ethanol in droplets with a limit of resolution of ∼0.5% ethanol by volume, corresponding to ∼0.4 mN/m in terms of surface tension (42). Such a change in surface tension measured by contact angle goniometry will occur at SDS concentrations exceeding hundreds of micromolars—three orders of magnitude higher than with the presented approach.

Next, we consider possible physical reasons to explain why we observe a decrease in $F_{pinning}$ at such low concentrations of SDS. The force of static friction acting on water droplets on a lubricated surface can be written as (41)

$$F_{pinning} = w(\gamma_{water-silicone\,oil} + \gamma_{air-silicone\,oil}) \cdot (\cos\theta_{rec} - \cos\theta_{adv}) \quad [1]$$

where $\gamma_{water-silicone\ oil}$ is the water–silicone oil interfacial tension, $\gamma_{air-silicone\ oil}$ is the air–silicone oil interfacial tension, w is the base width of the aqueous droplets at the surface, and θ_{adv} and θ_{rec} are the apparent advancing and receding contact angles, respectively. We note here that Eq. 1 considers $\gamma_{water-silicone\ oil}$ and $\gamma_{air-silicone\ oil}$ instead of the air–water surface tension due to the formation of a silicone oil–wrapping layer around the aqueous droplet at the silicone oil–infused micropillar surfaces (see *SI Appendix* and *SI Appendix*, Fig. S4) (39).

According to Eq. 1, three possible mechanisms exist for the observed decrease in $F_{pinning}$ of SDS aqueous droplets at silicone oil–infused micropillar-structured surfaces: (1) SDS decreases $\gamma_{water-silicone\ oil}$, (2) SDS decreases w, or (3) SDS decreases contact angle hysteresis (CAH = $\cos\theta_{rec} - \cos\theta_{adv}$). However, at low concentrations of SDS (in the range of 10 nM–10 μM), we observed no significant change in either the apparent contact angles or w of droplets on silicone oil–infused micropillar arrays (*SI Appendix*, Fig. S5), $\gamma_{water-silicone\ oil}$ (*SI Appendix*, Fig. S6), or the surface tension of the SDS aqueous phase (*SI Appendix*, Fig. S7). Based on these observations, and considering that CAH and the consequent $F_{pinning}$ of the contact lines at the surface is closely related to local surface roughness under the contact line of the droplet (43), we rule out possibilities (1) and (2). Thus, we hypothesize that the decrease in $F_{pinning}$ at ultralow concentration of SDS occurs because SDS decreases CAH. To support this hypothesis, we show in Fig. 2*B* that $F_{pinning}$ remains constant with different SDS

concentrations (0.1 nM–0.1 mM) on a flat DMOAP SAM-functionalized, silicone oil–coated Si wafer (*SI Appendix*, Fig. S8) and a conventional Krytox 103 perfluoropolyether oil–based SLIPS (see Materials and Methods; we note that water droplets cannot displace the lubricant to wet the micropillar edges in a conventional SLIPS, where water droplets are never in contact with the solid substrate). These results indicate that the self-assembly of SDS within the disordered DMOAP SAM at the outer edge of the top face of the micropillars plays an essential role in the observed SDS concentration–dependent F_{pinning}. Moreover, as shown in *SI Appendix*, Fig. S9 and discussed in the *SI Appendix*, imperfections in the DMOAP monolayer introduced by different methods likewise allow aqueous droplets to exhibit an SDS concentration–dependent F_{pinning} on DMOAP-functionalized surfaces.

Therefore, we reason that the nanoscopic environment created by the self-assembly of SDS within disordered DMOAP decreases the corresponding F_{pinning} of water droplets at the surfaces by locally concentrating amphiphilic analytes and smoothing the molecular roughness at the top edges of the micropillars. Moreover, we note that the presence of a threshold concentration of amphiphiles that triggers a measurable change in F_{pinning} (i.e., ~100 nM for SDS) hints at a signature of cooperative molecular assembly, which requires the participation of a threshold number of molecular building blocks and serves as the mechanism to drive the local accumulation of amphiphiles. This process shows striking similarities to the behavior of surfactant–polymer association in aqueous solutions (44–48). In an aqueous solution containing hydrophobically modified polymers, amphiphilic molecules can bind cooperatively to the hydrophobic regions of polymers to form surfactant–polymer complexes, resulting in a critical association concentration (CAC) that is lower than the CMC of the amphiphile alone (44–48). In our system, the loosely packed DMOAP SAM at the top edge of the micropillars plays a role that is analogous to the hydrophobically modified polymer: amphiphiles can cooperatively associate with the disordered DMOAP SAMs to alter the local surface roughness. The standard free energy changes accompanying the association of one amphiphile molecule from the bulk aqueous phase to the assembled state can be calculated using $\Delta G^0 = k_B T \ln(x_{\text{CAC}})$. By taking SDS as an example (CAC of ~100 nM based on Fig. 2*B*), we estimate ΔG^0 of SDS to be –20 $k_B T$.

To describe the essential change in the concentration-dependent water droplet mobility shown in Fig. 2*B*, we modified a classical model of cooperative association of surfactants and polymers (see *SI Appendix* for detailed derivations). The moles of amphiphiles in singly dispersed and micropillar-templated assembled states can be estimated by the following:

$$[X_{\text{total}}] = [X_{\text{monomeric}}] + [X_{\text{assembly}}] = [X_{\text{monomeric}}] + \sum_{i=1}^{N} \frac{[X_{\text{assembly}}]}{N} \frac{K_i [X_{\text{monomeric}}]^M}{1 + K_i [X_{\text{monomeric}}]^M} \quad [2]$$

where M is the aggregation number of assemblies of DMOAP and SDS, K_i is the corresponding intrinsic equilibrium constant for the self-assembly of amphiphiles at the disordered region of the DMOAP SAM, and X_{total}, $X_{\text{monomeric}}$, and X_{assembly} are the numbers of total amphiphiles, individually dispersed (monomeric) amphiphiles, and assembled amphiphiles within a 2-μL aqueous droplet on our surfaces, respectively. Taking SDS as an example, our thermodynamic model predicts an increase in $X_{\text{monomeric}}$ with X_{total}, suggesting that the majority of the SDS molecules remain singly dispersed in the bulk aqueous droplet below the CMC of SDS (Fig. 2*C*). In contrast, the model predicts an increase in X_{assembly} above the CAC (i.e., 100 nM) until the disordered SAM of DMOAP at the outer edge of the top face of the micropillars is fully occupied, as shown in Fig. 2*D*. This calculation suggests that the nanoscopic environment created by the disordered SAM region can direct the cooperative assembly and effective concentration of SDS molecules with the loosely packed DMOAP molecules, thus reducing the local disorder and roughness even at extremely low concentrations, without triggering any changes to the overall surface tension of the aqueous droplets, as schematically illustrated in Fig. 2*E*.

If this proposed mechanism is correct, then surfactants with head groups that are comparable to the tail length of DMOAP are expected to generate local disorder similar to that of the original SAM (see Fig. 3*A*) and hence should not change F_{pinning}. This reasoning is consistent with our measurements of F_{pinning} of aqueous droplets containing various concentrations of a nonionic synthetic surfactant, polyethylene glycol oleyl ether (Brij 97; head and tail lengths of 37.9 and 21.2 Å, respectively). As shown in Fig. 3*B*, we found that F_{pinning} of aqueous droplets containing Brij 97 remained constant over a wide range of concentrations (0.1 nM–10 μM). Similar phenomena were observed for a zwitterionic phospholipid, 1-palmitoyl-sn-glycero-3-phosphocholine (PGP), as shown in *SI Appendix*, Fig. S10. This amphiphile-dependent behavior suggests that unlike surface tension-based sensors, our platform shows promise in distinguishing amphiphiles with different chemical structures at low concentrations.

Even more interesting, we find that amphiphiles that are significantly larger than DMOAP increase the F_{pinning} of water droplets, a completely opposite trend compared to the case of SDS, but still explainable by the same cooperative assembly mechanism schematically shown in Fig. 3*C*. We observed this behavior upon measuring F_{pinning} of phosphate-buffered saline (PBS) aqueous droplets containing pathogenic, amphiphilic endotoxins, which are commonly used as biomarkers for environmental and health monitoring. Endotoxins are composed of large lipopolysaccharides consisting of a lipid A covalently bonded to a high-molecular-weight polysaccharide head group (Fig. 3*C*) and tend to show toxicity at extremely low concentrations (~2 ng/mL) (14, 15). Therefore, no wettability-based assay has ever achieved their ultrasensitive detection in biologically or environmentally relevant concentrations. In contrast, our method begins to show a measurable increase in F_{pinning} at endotoxin concentrations as low as 1 ng/mL, a sufficiently low limit that offers a useful and convenient method for on-site environmental monitoring (e.g., in water containing harmful algal blooms with 2 ng/mL endotoxin (14)).

To provide insights to the mechanism by which endotoxin increases F_{pinning}, we further tested F_{pinning} of aqueous droplets containing either polysaccharide or lipid A, two components of endotoxin (Fig. 3*D*). Although F_{pinning} of droplets containing polysaccharide increases as the concentration of polysaccharide increases, the detection threshold concentration for polysaccharide (10 μg/mL) is ~4 orders of magnitude higher than that of endotoxin (1 ng/mL). On the contrary, while the F_{pinning} of aqueous droplets of lipid A decreased with the increase in the concentration of lipid A, the threshold concentration of lipid A was observed to be the same as endotoxin. These results led us to hypothesize that the hydrophobic lipid part of the endotoxin molecules is essential in driving the partition and local concentration of endotoxins to loosely packed regions of the DMOAP SAM at the outer edge of the top face of the micropillars, whereas the high-molecular-weight, hydrophilic polysaccharide groups may greatly increase the local roughness of the disordered SAM

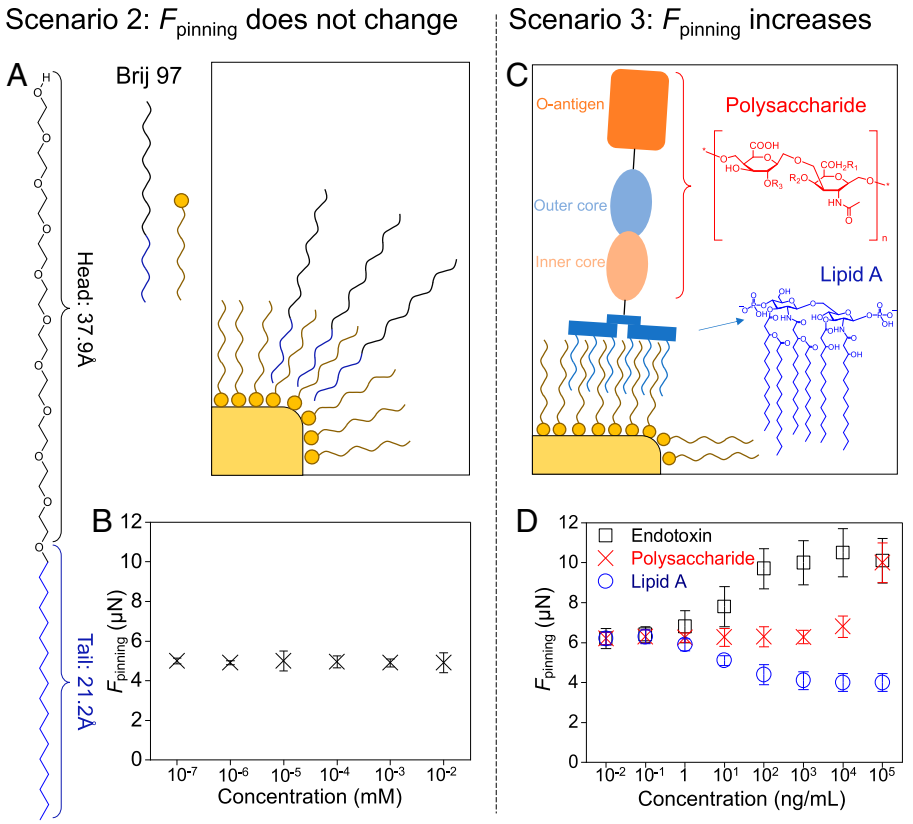

Fig. 3. (*A*) Molecular structure of a nonionic amphiphile, Brij 97, and a scheme of coassembly of Brij 97 at the disordered DMOAP SAM region. Note that Brij 97 is nearly twice as long as the length of DMOAP. The length of Brij was calculated from Chem3D. The structure of the SAM is schematic. (*B*) $F_{pinning}$ of aqueous droplets on a DMOAP-functionalized Si micropillar array lubricated with silicone oil as a function of Brij 97 concentration. (*C*) Molecular structure of an endotoxin molecule, which consists of a lipid A covalently bound to a polysaccharide head group. The polysaccharide is composed of O-antigen, outer core, and inner core segments, which are linearly and covalently bound. Note that endotoxin is much larger than DMOAP, the scheme in (*C*) is not to scale, and the structure of the SAM is schematic. (*D*) $F_{pinning}$ of aqueous droplets on a DMOAP SAM-functionalized silicon micropillar array lubricated with silicone oil as a function of concentrations of endotoxin, lipid A, and polysaccharide. The volume of aqueous droplets is kept at 2 μL.

and the consequent $F_{pinning}$ of the aqueous droplets at DMOAP SAM-functionalized, silicone oil–infused Si micropillar arrays.

In our final set of experiments, we used this analyte concentrator–driven chemical detection to build a proof-of-concept device composed of different micropillar structures to sort water samples into discrete groups based on their amphiphile concentrations. Fig. 4*A* confirms that for aqueous droplets with a given SDS concentration, the $F_{pinning}$ increases linearly with the total circumference of micropillars around the receding front of the water droplet at our system (C_{tot}; the total surface area of underlying micropillars [A_{tot}] was held constant by varying both P and R of the micropillars, as described in the *SI Appendix*). Furthermore, as described in Fig. 4*B* and the *SI Appendix*, $F_{pinning}$ was found to be independent of A_{tot} while holding C_{tot} constant.

Using these results, we designed and fabricated a DMOAP SAM-functionalized, silicone oil–infused microstructured surface composed of 5 distinct regions of micropillars. The radii of the micropillars were identical in all 5 regions, while the P between micropillars of each region varied from 35 μm at the top region to 15 μm at the bottom region. As $F_{pinning} \propto C_{tot} \propto P^{-1}$, each region had an associated threshold concentration of surfactants below which aqueous droplets became pinned when the surface was tilted at a fixed inclination angle. Since each region offers a unique threshold concentration, droplets can be sorted into discrete groups with upper and lower limits corresponding to threshold concentrations of consecutive regions. To demonstrate this principle, we placed aqueous droplets with SDS concentrations ranging from 0.1 to 100 μM in the region with $P = 35$ μm (smallest $F_{pinning}$). As the wafer was inclined to ∼6°, droplets with higher concentrations of SDS became pinned to regions with lower values of P, thus allowing simple sorting of aqueous droplets based on SDS concentration (Fig. 4*C* and *SI Appendix*, Movie S1). Overall, this result provides proof of concept for the design of laboratory-on-a-chip surfaces that can offer design principles for sensing and sorting aqueous droplets based on cooperative association between amphiphiles and disordered DMOAP SAMs with an extremely high sensitivity.

Conclusions

In this work, we have developed surfaces composed of DMOAP SAM-functionalized Si micropillar arrays lubricated with silicone oil that can effectively concentrate trace amounts of amphiphiles locally at the disordered regions of SAM and thus enable their ultrasensitive detection (five orders of magnitude below the CMC of SDS and at environmentally relevant endotoxin concentrations) by visually monitoring the sliding characteristics of aqueous droplets. Our surfaces provide a rapid and portable method of detecting amphiphiles within microliter-scale relatively pure droplets (e.g., endotoxins in sterile water) without the use of specialized equipment. (We note that this method is not applicable as described for the analysis of target molecules in complex mixtures due to the presence of potential interferents.) Unlike surface tension–based techniques, this platform is based on the design principle of concentrating amphiphiles within the disordered

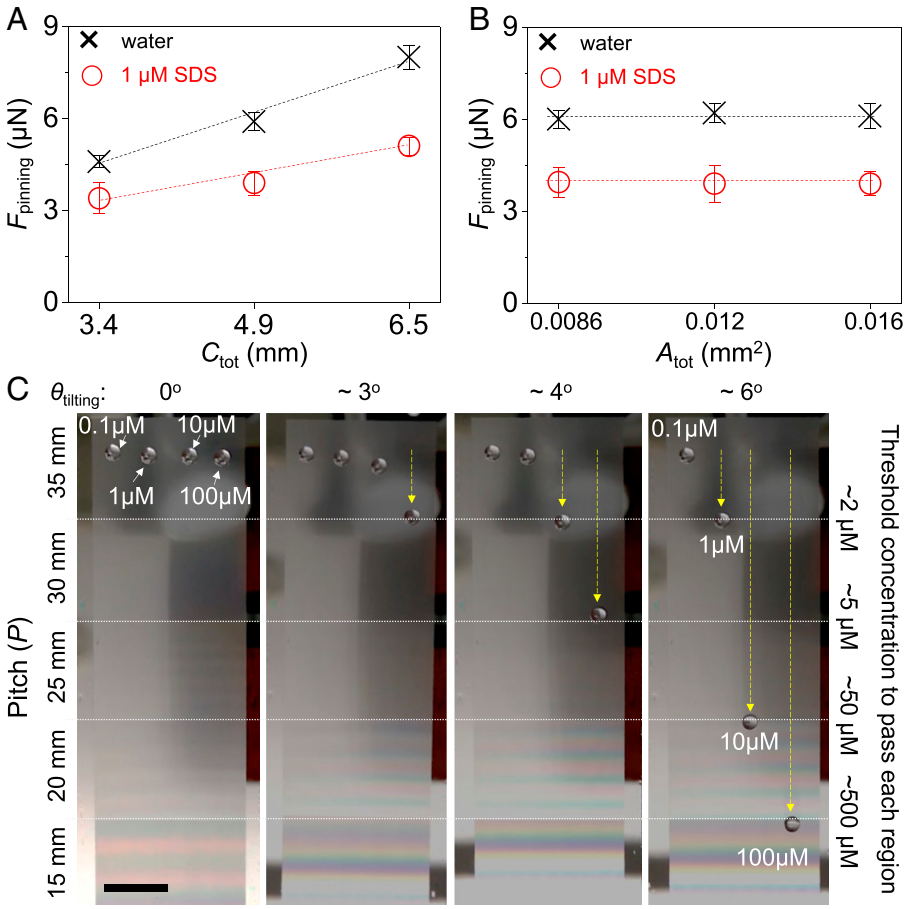

Fig. 4. Sorting SDS-laden aqueous droplets into discrete groups using a patterned lubricated DMOAP-functionalized Si micropillar array. Plot showing $F_{pinning}$ of aqueous droplets as a function of (*A*) total circumference (C_{tot}) and (*B*) total surface area (A_{tot}) of the total micropillars under water droplets. (*C*) Sequential photographs showing pinning of SDS-laden aqueous droplets on a DMOAP SAM-functionalized Si micropillar array lubricated with silicone oil with a gradient in micropillar dimensions. *P* was varied from 35 to 15 μm (from *top* to *bottom*), while *R* remained constant at 5 μm in each region. Threshold SDS concentrations for aqueous droplets to pass different regions are listed next to the photographs. The volume of SDS aqueous droplets was 2 μL. Scale bar, 1 cm.

SAM by cooperative assembly. Because the disordered region of our SAMs coincides with the location of the contact line of the droplet, minute concentrations of amphiphiles can effectively change the mobilities of droplets, even when bulk surface properties of the droplet (e.g., surface tension) remain unchanged. We also developed a thermodynamic model that captures the salient features of the cooperative assembly mechanism and demonstrated a laboratory-on-a-chip device to easily sort droplets with different concentrations of SDS by pinning them to specific locations on the functional surface. Moreover, our platform shows great potential for cost-effective and rapid detection of a bacterial amphiphile, endotoxin, for early disease diagnostics and environmental water quality monitoring. Furthermore, the coassembly behavior of amphiphilic analytes with SAMs and the resulting analyte concentration effects can be finely tuned by changing the sizes of the hydrophobic and hydrophilic blocks in the SAM molecules relative to those of the target amphiphile to achieve desired wetting behavior and local surface properties. Although in this work we focus on the changes in pinning forces, the process of concentrating amphiphilic analytes in loosely packed SAMs is generalizable and can be used to enhance the sensitivity of other detection techniques. For instance, our results in Fig. 1*C* illustrate that fluorescent analytes become concentrated on the edges of micropillars, suggesting that this phenomenon lowers the minimum bulk concentration at which these analytes can be detected using fluorescent imaging. We anticipate that other detection techniques could likewise benefit from analytes being concentrated into select regions. Future efforts seek to provide detailed nanoscopic structures of the imperfections in SAMs for amphiphile self-assembly.

Materials and Methods

Materials. The following chemicals were purchased from Sigma-Aldrich: SDS, CTAB, Brij 97, PGP, endotoxin (from *Escherichia coli* O111:B4, ~45,000 g/mol), lipid A, polysaccharide (molecular weight of ~40,000 g/mol), DMOAP (42 wt% in methanol), BODIPY-labeled fatty acid, PBS, and silicone oil (10 cSt). Krytox 103 perfluoropolyether oil was obtained from DuPont. Anhydrous ethanol was obtained from Decon Labs. Purchased chemicals were used as received without further modification or purification. Deionized water used in this work was obtained from a Milli-Q water purification system (Simplicity C9210). Si wafers were purchased from Nova Electronic Materials.

Fabrication of Micropillar Arrays on Si Wafers. Designed micropillar arrays were fabricated through photolithography and deep ion etching. Photoresist (SPR220-4.5) was first spin coated on Si wafers and patterned under ultraviolet (UV) exposure by the Heidelberg MLA150 Maskless Aligner. The resulting photoresist patterns were used as masks to perform deep ion etching of the underlying Si water with an STS-inductively coupled plasma reactor-reactive ion etch system to fabricate designed micropillar arrays. The Si wafer was then cleaned with acetone and oxygen plasma treatment to remove the residual photoresist. The fabricated Si micropillars were characterized using a Zeiss Ultra Plus field emission scanning electron microscope.

DMOAP Functionalization of Si Wafer. First, Si wafers were rinsed with a copious amount of water and ethanol and dried under a stream of nitrogen gas before being treated with oxygen plasma for 1 h. Second, the cleaned Si wafers were placed in 1% vol/vol DMOAP aqueous solution (∼150 mL) for 10 min. Third, the Si wafers were washed with water and ethanol to remove the unreacted and loosely held DMOAP molecules and were subsequently dried under nitrogen gas. The resultant DMOAP SAMs had a low roughness of ∼0.1 nm (*SI Appendix*, Fig. S10). These DMOAP functionalized Si wafers were stored in dark, ambient conditions until further use to prevent the damage caused by DMOAP functionalization under light exposure.

Preparation of Perfluorinated Oil–Based SLIPS Using Si Wafers. First, Si wafers were rinsed with a copious amount of water and ethanol before a final rinse with acetone, after which the wafer was dried under a stream of nitrogen gas and treated with oxygen plasma for 1 h. Second, the precleaned Si wafers were placed in a vacuum chamber and functionalized by flowing poly(C_4F_8) under vacuum with radiofrequency plasma for 8 s. Poly(C_4F_8)-functionalized Si wafers were stored in dark, ambient conditions until further use to prevent the damage of C_4F_8 functionalization under light exposure. The microstructures were infused with Krytox 103, a perfluorinated oil, before use.

Infusion of Silicone Oil into Micropillar-Structured and Flat Si Wafers. Silicone oil (10 cSt) was infused into DMOAP functionalized micropillar-structured Si wafers by spin coating at 350 rpm for 4.5 min (ramp time: 10 s). Flat Si wafers were coated in silicone oil by spin coating at 1,000 rpm for 2 min (ramp time: 10 s).

Goniometer Measurements. A goniometer (KRUSS DSA 100) was used to measure the contact angles of water droplets on silicone oil–infused micropillar-structured Si wafers. These measurements were performed using the sessile drop mode. Surface tensions (silicone oil–water, air–silicone oil, and air–water) were measured using the pendant method. For the silicone oil–water interfacial tension measurement, water was placed inside a quartz cuvette and the silicone oil was placed in a syringe with a needle tip held under the water surface. A high-resolution camera attached onto the goniometer was used to capture the images and built-in software was used to calculate the interfacial tension. For sliding angle measurements, we placed a 2-μL water droplet on the goniometer stage and tilted the surface at the rate of ∼5°/min using the built-in software. The angle at which the droplet started to slide was recorded as its sliding angle.

Friction Force Analysis. The forces of friction acting on droplets sliding across our surfaces were measured using a custom-built cantilever setup. The cantilever was built from an acrylic needle with inner and outer diameters of 189 and 250 μm, respectively, and whose openings were sealed with a UV-curable epoxy. The cantilever was mounted on the goniometer, and droplets were adhered to the side of the cantilever. A rotating stage (ThorsLabs PRM1Z8 brushless DC motor) rotated the substrate with an angular velocity of 1°/s, where the droplet was positioned ∼5.7 cm away from the center of rotation. When the stage was rotated, the needle was deflected from its equilibrium position, resulting in a change in its position (Δx). This entire process was recorded on video and then processed through the software *Tracker* to extract Δx as a function of time. F_d was calculated as

$$F_d = k\Delta x \quad [3]$$

where k was the spring constant of the needle, which was measured by placing droplets of different volumes on the capillary tube positioned horizontally, and the deflection of the needle in the z direction was measured. $F_{pinning}$ was recorded as the maximum F_d before either a gradual or abrupt decline in F_d as a function of time. If multiple peaks were present (e.g., due to repinning events), then $F_{pinning}$ was recorded as the first major decline in F_d. The k values of cantilevers used in this study were ∼10 mN/m.

To avoid contamination when working with low concentrations of amphiphiles, serial dilutions of amphiphiles were carefully prepared in glass vials that had been thrice rinsed with Milli-Q water. When measuring $F_{pinning}$ as a function of the concentration of amphiphiles, concentrations were tested in ascending order (i.e., lowest to highest concentration). In addition, droplets of different amphiphile concentrations were either tested in different regions of the silicone oil–infused or DMOAP SAM-functionalized microstructured Si wafer, or the wafer was cleaned with ethanol and respin coated before testing droplets with different concentrations.

Wrapping Layer of Aqueous Droplets at Silicone Oil–Infused Micropillar-Structured Substrate. We imaged the wrapping layer on the aqueous droplet resting upon a silicone oil–infused micropillar-structured substrate using a custom-made color interferometer (see *SI Appendix*). We illuminated a 2-μL water droplet using diffuse white light-emitting diodes, and the interference patterns were captured using a Canon digital single-lens reflex camera.

Fluorescence Microscopy Imaging of BODIPY-Labeled Amphiphiles on Silicone Oil–Infused Micropillar-Structured Substrate. We prepared 1 μg/mL BODIPY-labeled fatty acid aqueous solution and placed 10 μL of the obtained solution on the DMOAP SAM-functionalized micropillar-structured Si wafer covered with silicone oil. Next, we used an Olympus IX73 fluorescence microscope to image the distribution of BODIPY-labeled fatty acids at the surface of DMOAP SAM-functionalized micropillar-structured Si wafer.

Data Availability. All of the study data are included in the article and/or supporting information.

ACKNOWLEDGMENTS. This research was supported by the NSF through the Harvard University Materials Research Science and Engineering Center (DMR-2011754). We thank Dr. M. Aizenberg and Prof. Paul S. Weiss for constructive feedback and comments.

Author affiliations: [a]Department of Chemistry and Chemical Biology, Harvard University, Cambridge, MA 02138; [b]John A. Paulson School of Engineering and Applied Sciences, Harvard University, Cambridge, MA 02138; [c]William G. Lowrie Department of Chemical and Biomolecular Engineering, The Ohio State University, Columbus, OH 43210; [d]Division of Physical Sciences and Engineering, King Abdullah University of Science and Technology (KAUST), Thuwal, 23955, Saudi Arabia; and [e]Sustainability Institute, The Ohio State University, Columbus, OH 43210

Author contributions: Y.Y., R.K.A.B., J.A., and X.W. designed research; Y.Y., R.K.A.B., Y.X., A.M.R., S.L., T.C.C., A.B., M.J.K., and X.W. performed research; D.D. and S.A. contributed new reagents/analytic tools; Y.Y., R.K.A.B., M.J.K., D.D., S.A., J.A., and X.W. analyzed data; and Y.Y., R.K.A.B., J.A., and X.W. wrote the paper.

1. J. Z. Kubicek-Sutherland, D. M. Vu, H. M. Mendez, S. Jakhar, H. Mukundan, Detection of lipid and amphiphilic biomarkers for disease diagnostics. *Biosensors (Basel)* **7**, 25 (2017).
2. V. E. Yushmanov, J. R. Perussi, H. Imasato, M. Tabak, Interaction of papaverine with micelles of surfactants with different charge studied by 1H-NMR. *Biochim. Biophys. Acta* **1189**, 74–80 (1994).
3. E. Olkowska, Ż. Polkowska, J. Namieśnik, Analytics of surfactants in the environment: Problems and challenges. *Chem. Rev.* **111**, 5667–5700 (2011).
4. T. Cserháti, E. Forgács, G. Oros, Biological activity and environmental impact of anionic surfactants. *Environ. Int.* **28**, 337–348 (2002).
5. M. Lechuga, M. Fernández-Serrano, E. Jurado, J. Núñez-Olea, F. Ríos, Acute toxicity of anionic and non-ionic surfactants to aquatic organisms. *Ecotoxicol. Environ. Saf.* **125**, 1–8 (2016).
6. T. Ivanković, J. Hrenović, Surfactants in the environment. *Arh. Hig. Rada Toksikol.* **61**, 95–110 (2010).
7. S. D. Lawn, A. D. Kerkhoff, M. Vogt, R. Wood, Diagnostic accuracy of a low-cost, urine antigen, point-of-care screening assay for HIV-associated pulmonary tuberculosis before antiretroviral therapy: A descriptive study. *Lancet Infect. Dis.* **12**, 201–209 (2012).
8. J. Minion *et al.*, Diagnosing tuberculosis with urine lipoarabinomannan: Systematic review and meta-analysis. *Eur. Respir. J.* **38**, 1398–1405 (2011).
9. H. Jiang, J. Yang, K. Wan, D. Jiang, C. Jin, Miniaturized paper-supported 3D cell-based electrochemical sensor for bacterial lipopolysaccharide detection. *ACS Sens.* **5**, 1325–1335 (2020).
10. M. B. Linder, G. R. Szilvay, T. Nakari-Setälä, M. E. Penttilä, Hydrophobins: The protein-amphiphiles of filamentous fungi. *FEMS Microbiol. Rev.* **29**, 877–896 (2005).
11. N. Österlund *et al.*, Amyloid-β peptide interactions with amphiphilic surfactants: Electrostatic and hydrophobic effects. *ACS Chem. Neurosci.* **9**, 1680–1692 (2018).
12. P. Sondhi, M. H. U. Maruf, K. J. Stine, Nanomaterials for biosensing lipopolysaccharide. *Biosensors (Basel)* **10**, 2 (2019).
13. O.-P. Kallioniemi *et al.*, Serum CA 15-3 assay in the diagnosis and follow-up of breast cancer. *Br. J. Cancer* **58**, 213–215 (1988).
14. J. Rapala *et al.*, Endotoxins associated with cyanobacteria and their removal during drinking water treatment. *Water Res.* **36**, 2627–2635 (2002).
15. J. Cohen, The immunopathogenesis of sepsis. *Nature* **420**, 885–891 (2002).
16. R. Gorman, Atlantic horseshoe crabs and endotoxin testing: Perspectives on alternatives, sustainable methods, and the 3Rs (replacement, reduction, and refinement). *Front. Mar. Sci.* **7**, 582132 (2020).
17. I.-H. Lin *et al.*, Endotoxin-induced structural transformations in liquid crystalline droplets. *Science* **332**, 1297–1300 (2011).
18. Y. Y. Goh, V. Frecer, B. Ho, J. L. Ding, Rational design of green fluorescent protein mutants as biosensor for bacterial endotoxin. *Protein Eng.* **15**, 493–502 (2002).
19. M. K. McCamley, A. W. Artenstein, S. M. Opal, G. P. Crawford, Optical detection of sepsis markers using liquid crystal based biosensors. *Proc. SPIE* **6441**, 64411Y (2007).

20. E. Bukusoglu, M. Bedolla Pantoja, P. C. Mushenheim, X. Wang, N. L. Abbott, Design of responsive and active (soft) materials using liquid crystals. *Annu. Rev. Chem. Biomol. Eng.* **7**, 163–196 (2016).
21. S. Movafaghi *et al.*, Tunable superomniphobic surfaces for sorting droplets by surface tension. *Lab Chip* **16**, 3204–3209 (2016).
22. Z. Chu, S. Seeger, Superamphiphobic surfaces. *Chem. Soc. Rev.* **43**, 2784–2798 (2014).
23. L. Wen, Y. Tian, L. Jiang, Bioinspired super-wettability from fundamental research to practical applications. *Angew. Chem. Int. Ed. Engl.* **54**, 3387–3399 (2015).
24. R. Mohammadi, J. Wassink, A. Amirfazli, Effect of surfactants on wetting of super-hydrophobic surfaces. *Langmuir* **20**, 9657–9662 (2004).
25. N. C. Santos, A. C. Silva, M. A. R. B. Castanho, J. Martins-Silva, C. Saldanha, Evaluation of lipopolysaccharide aggregation by light scattering spectroscopy. *ChemBioChem* **4**, 96–100 (2003).
26. D. Quéré, Wetting and roughness. *Annu. Rev. Mater. Res.* **38**, 71–99 (2008).
27. J. N. Israelachvili, *Intermolecular and Surface Forces* (Elsevier, New York, ed. 3, 2011), pp. 469–499.
28. M. Nosonovsky, B. Bhushan, Biologically inspired surfaces: Broadening the scope of roughness. *Adv. Funct. Mater.* **18**, 843–855 (2008).
29. W. Xu, C.-H. Choi, From sticky to slippery droplets: Dynamics of contact line depinning on superhydrophobic surfaces. *Phys. Rev. Lett.* **109**, 024504 (2012).
30. C. Huh, L. E. Scriven, Hydrodynamic model of steady movement of a solid/liquid/fluid contact line. *J. Colloid Interface Sci.* **35**, 85–101 (1971).
31. P. G. de Gennes, Soft matter. *Science* **256**, 495–497 (1992).
32. J. Aizenberg, A. J. Black, G. M. Whitesides, Controlling local disorder in self-assembled monolayers by patterning the topography of their metallic supports. *Nature* **394**, 868–871 (1998).
33. A. J. Black, K. E. Paul, J. Aizenberg, G. M. Whitesides, Patterning disorder in monolayer resists for the fabrication of sub-100-nm structures in silver, gold, silicon, and aluminum. *J. Am. Chem. Soc.* **121**, 8356–8365 (1999).
34. D. K. Schwartz, Mechanisms and kinetics of self-assembled monolayer formation. *Annu. Rev. Phys. Chem.* **52**, 107–137 (2001).
35. T. J. Mullen, A. A. Dameron, H. M. Saavedra, M. E. Williams, P. S. Weiss, Dynamics of solution displacement in 1-adamantanethiolate self-assembled monolayers. *J. Phys. Chem. C* **111**, 6740–6746 (2007).
36. S. A. Claridge *et al.*, From the bottom up: Dimensional control and characterization in molecular monolayers. *Chem. Soc. Rev.* **42**, 2725–2745 (2013).
37. M. Kim, J. N. Hohman, E. I. Morin, T. A. Daniel, P. S. Weiss, Self-assembled monolayers of 2-adamantanethiol on Au111: Control of structure and displacement. *J. Phys. Chem. A* **113**, 3895–3903 (2009).
38. T.-S. Wong *et al.*, Bioinspired self-repairing slippery surfaces with pressure-stable omniphobicity. *Nature* **477**, 443–447 (2011).
39. D. Daniel, J. V. I. Timonen, R. Li, S. J. Velling, J. Aizenberg, Oleoplaning droplets on lubricated surfaces. *Nat. Phys.* **13**, 1020–1025 (2017).
40. N. Gao *et al.*, How drops start sliding over solid surfaces. *Nat. Phys.* **14**, 191–196 (2018).
41. D. Daniel *et al.*, Origins of extreme liquid repellency on structured, flat, and lubricated hydrophobic surfaces. *Phys. Rev. Lett.* **120**, 244503 (2018).
42. E. J. Falde, J. Wang, M. W. Grinstaff, Surface tension sensor meshes for rapid alcohol quantification. *RSC Adv.* **7**, 49795–49798 (2017).
43. L. Wang, T. J. McCarthy, Covalently attached liquids: Instant omniphobic surfaces with unprecedented repellency. *Angew. Chem. Int. Ed. Engl.* **55**, 244–248 (2016).
44. A. Yekta, J. Duhamel, P. Brochard, H. Adiwidjaja, M. A. Winnik, A fluorescent probe study of micelle-like cluster formation in aqueous solutions of hydrophobically modified poly(ethylene oxide). *Macromolecules* **26**, 1829–1836 (1993).
45. S. Biggs, J. Selb, F. Candau, Effect of surfactant on the solution properties of hydrophobically modified polyacrylamide. *Langmuir* **8**, 838–847 (1992).
46. R. Tanaka, J. Meadows, P. A. Williams, G. O. Phillips, Interaction of hydrophobically modified hydroxyethyl cellulose with various added surfactants. *Macromolecules* **25**, 1304–1310 (1992).
47. F. Guillemet, L. Piculell, Interactions in aqueous mixtures of hydrophobically modified polyelectrolyte and oppositely charged surfactant. Mixed micelle formation and associative phase separation. *J. Phys. Chem.* **99**, 9201–9209 (1995).
48. L. Piculell, F. Guillemet, K. Thuresson, V. Shubin, O. Ericsson, Binding of surfactants to hydrophobically modified polymers. *Adv Colloid Interface* **63**, 1–21 (1996).